Optimal tool orientation in 3 + 2-axis machining considering machine kinematics

Laureen Grandguillaume, Sylvain Lavernhe, Christophe Tournier

Optimal tool orientation in 3+2 -axis machining considering machine kinematics

Laureen Grandguillaume · Sylvain Lavernhe · Christophe Tournier

Received: xxxx / Accepted: xxxx

Abstract In 5-axis machining, the initial orientation and position of the part in the fixture on the machine table are chosen to avoid collisions and to ensure that axes ranges are respected. However, kinematics of the machine is rarely considered for workpiece setup optimization although it affects the tool path execution and machining time. Indeed, for complex surfaces, actual feedrate is often lower than the programmed one and can present strong slowdowns, which are critical for the tool cutting conditions and therefore the part quality. This article investigates the use of kinematic manipulability criteria to determine the best orientation of the workpiece setup to maximize the actual feedrate and reduce machining time. The modelling of maximum velocity, acceleration and jerk of each axis by means of polytopes makes it possible to take advantage of the whole kinematic space of the machine more intuitively. Simulations and experiments are carried out in 3+2-axis machining on test parts with a ball-end tool. For stretched surfaces, while the tool center motion is given by the machining strategy, the tool axis orientation is optimized jointly with the workpiece setup. Experiments confirm that actual feedrate raises faster to better respect the programmed cutting conditions along each path. As feedrate is also higher, machining time is reduced significantly.

Keywords High Speed Machining · Workpiece setup · Kinematics · Polytope · Manipulability

L. Grandguillaume, S. Lavernhe, C. Tournier
Université Paris-Saclay, ENS Paris-Saclay, LURPA, 91190 Gif-sur-Yvettes, France
E-mail: sylvain.lavernhe@ens-paris-saclay.fr

1 Introduction

Machining complex parts in 3-axis machining may require different workpiece setups to machine the part entirely while avoiding local collision with the tool and global collisions between part, clamping system, tool holder, and more generally with any machine component and intrusive device. To maximize productivity by reducing successive setups, previous works focus on determining optimal workpiece position and/or orientation on the machine table to increase the number of faces which can be machined in one single setup. Hence several heuristic solutions, based on geometrical criteria like accessibility, lead to an optimal number of setups to machine the part completely [1–4].

On the one hand, the use of 5-axis machining allows to increase productivity by reducing the number of part setups. On the other hand, tool paths can be optimized relatively to the local shape and curvature of the part, but it requires a better expertise than 3-axis. Indeed, the whole process should be considered to achieve efficient multi-axis machining. For that purpose, different developments in the literature focus on adapting performance improvement to a specific type of parts. It is possible to choose adapted machining strategy, machine tool and workpiece setup.
Briefly, most of research articles deal with the tool path (i.e., tool tip position and tool axis orientation relatively to the part) to increase the machining efficiency based on the material removal rate criterion. Chiou et al. compute a trajectory based on a machining potential field to raise the machining strip width [5]. This field represents the optimal cutting direction at any point on the surface. Barakchi-Fard et al. also determine the feed direction and tool orientation to maximize the machining strip width [6].

Such pure geometric criterion does not take into account the machine kinematics and can lead to dramatic feedrate drops that mark the workpiece and then deteriorate the surface quality. High solicitations of machine axes, especially rotary axes, can slow down the actual feedrate compared with 3-axis machining [7]. To address that issue, actual machine tool behaviour is considered jointly to the geometrical problem. Kim et al. determine the tool path directions to achieve the best kinematic performances [8]. Farouki et al. consider the whole inverse kinematics of the machine along the tool path to compute an accurate and efficient 5-axis machining of free-form surfaces limiting the use of rotary axes [9]. More recently, Hu et al. present a relevant approach defining numerical estimations of velocity, acceleration and jerk of each axis for all feed directions. Hence they perform an intersection of machine's kinematic constraints to determine the maximal effective material removal rate [10].
From the machine tool point of view, pure kinematics study can help to design the process. Bohez classifies all possible designs of 5-axis machines thanks to quantitative parameters. Orientation space and angle index, efficiency of the machine tool space are defined to compare different architectures [11]. Tutunea-Fatan et al. recommend selecting the machine to minimize the total joint displacement using a generic kinematic model for a given tool path [12].

In this article, the emphasis is on the workpiece setup regarding the tool path and the machine tool. In literature, it is chosen according to different criteria mainly related to machining errors or machining time.

Concerning machining errors, Anotaipaiboon et al. show that the workpiece setup and the tool length have an influence [13]. The optimized setup is determined numerically by finding a position with the minimum non-linear error caused by the kinematic transformations for specific NC program and machine tool. Lin et al. propose to optimize the workpiece setup location in order to reduce the non-linear errors of 5-axis machining by the particle swarm optimization [14]. Recently Yang et al. determine the optimal placement for parts on 5-axis machines to minimize the tracking errors of servo drives under cutting loads [15].

Regarding machining time, the feedrate control is essential because it reflects directly the tool path performances as productivity. But actual feedrate at the tool tip also impacts the surface quality through the modification of the tool load and tool deflection due to variable chip thickness. The first type of method consists of a purely geometrical reasoning, independently of kinematic capacities of the axes. Both rotary and linear axes can be considered. Pessoles et al. propose to determine the orientation of the part while minimizing the total distance covered by rotary axes [16]. The selection of the part position is carried out by minimizing the total distance covered by linear axes. Therefore, this two-step approach significantly reduces all axes movements. In the same way, Shaw et al. base their method on the minimization of the displacement of the linear axes by finding the optimal position of the workpiece on the 5-axis machine table [17]. In fact, these two approaches are quite similar because the motion of the linear and rotary axes are coupled by the forward kinematics. Nevertheless, these purely geometrical methods tend to reduce the total machining time but do not prevent slowdowns of the actual feedrate, which generate marks on the part. The second type of method considers the kinematic capacities of the axes which correspond to the limits of the actuators, or the tuning of the axes parameters in the CNC (maximum feedrate, acceleration and jerk). These limits are taken into account during the interpolation of the tool path (feedrate planning) [18, 19]. The position setpoints for each physical axis are then kinematically compatible with the axis dynamics during the trajectory execution [20]. Hu et al. consider kinematics by finding a workpiece setup which reduces maximal angular accelerations of the rotary axes thanks to a genetic algorithm [21]. This method allows reducing acceleration constraints but it is not necessarily the limiting parameter to reach the programmed feedrate and thus to reduce machining time. Xu et al. and Campatelli et al. consider both velocity and acceleration of each axis to estimate the influence of the workpiece setup on the machining time [22, 23]. Those developed criteria reduce rotary axes movements because they often limit the actual feedrate experimentally. However, these studies do not combine axes performances. The three kinematic levels, i.e., velocity, acceleration and jerk are fundamental requirements for tool path interpolation and the inverse kinematics of the machine.

The general thematic addressed in this paper is the enhancement of the productivity of parts with complex surfaces. The developed works focus on the increase of the actual feedrate during the execution of trajectories by using the composition of the movement of the machine axes. In this sense, the manufacturing process of the part (excluding the trajectory) and the setup of the part in the machine workspace are assumed to be fixed and are not being questioned. It is thus a problem, for a given machine tool, i.e. its architecture and kinematics, to determine the best use of the axes that it is possible to make by the elaboration of a kinematically suitable

trajectory.
The overall problem, corresponding to the case of continuous 5-axis machining, consists in determining the path to be followed by the tool tip as well as the orientation of the tool axis. As seen throughout the literature review, this problem remains very open as it couples at the same time the design of the toolpath (position and orientation of the tool), the machine kinematic behaviour and the limited jerk interpolation. The aim in this paper is to adopt a kinematic modelling of machining centers that is as representative as possible of its true capabilities, without being restrictive, associated to a resolution method which maximize the relative workpiece-tool tip feedrate that can be reached along a path.
For this paper, the scope is restricted to 3+2 -axis machining where it is possible to modify the orientation of the tool axis for each path. Very few previous works address this problem. Zhu et al. propose an optimization method to determine the workpiece setup in 3+2 -axis in order to raise the width of the machined strip [24]. Yet, as the viewpoint is purely geometric, the material removal rate is not fully optimized because the feedrate is depending on axis performances and solicitations caused by the interpolation of the path.
In the aforementioned kinematic context, the objective is to take advantage of the dynamics of the translation axes by optimizing the choice of the relative tool-workpiece orientation. In this sense, 3+2 -axis machining can also be seen as an optimization of the workpiece setup, particularly by its orientation. The novelty of the works lies in the use of kinematic polytopes of velocity, acceleration and jerk as well as in the proposal of a formulation and resolution of the optimization problem. The results of the simulations are compared with measurements on an industrial machine to demonstrate the gain brought by such modelling and resolution.

The structure of the rest of the paper is as follows: in the second section, limiting parameters for the actual feedrate are presented, with both joint space and part space points of view. Then, section 3 deals with the model of kinematic manipulability polytopes used in this work. Based on these polytopes, a method is proposed to define the workpiece orientation in 3+2 -axis machining. Last section is dedicated to experiments on 5-axis milling center for two test parts to access the efficiency of the approach before concluding remarks.

2 Limiting parameters for the actual feedrate

2.1 Kinematic limits

Kinematic performances of machine tools are limited by the maximum velocity ($\dot{q}_i$), acceleration ($\ddot{q}_i$) and jerk ($\dddot{q}_i$) of each axis i, tuned in the CNC, considering motor performances and machine structure, in order to avoid vibrations and to obtain the required surface quality (Equation 1). Indeed, actuator torques are limited in order to eliminate highly jerky motions of axes [25], thus, jerk values are tuned for each axis given the machine tool structure behaviour.

$$\begin{cases} {\dot{q}_i}^{\min} \leqslant \dot{q}_i(t) \leqslant {\dot{q}_i}^{\max} \\ {\ddot{q}_i}^{\min} \leqslant \ddot{q}_i(t) \leqslant {\ddot{q}_i}^{\max} \\ {\dddot{q}_i}^{\min} \leqslant \dddot{q}_i(t) \leqslant {\dddot{q}_i}^{\max} \end{cases} \tag{1}$$

2.2 Jerk controlled movement law

The jerk controlled movement law defines a trapezoidal acceleration profile limited by jerk command. This kind of profile offers a continuous acceleration and reduces the magnitude of machine's structural vibrations. For a straight line, the duration of the tool tip displacement is the sum of seven local durations [26]. Figure 1 shows a kinematic profile for trapezoidal acceleration with the seven sequences. The higher the value of the jerk is, the smaller the motion time.

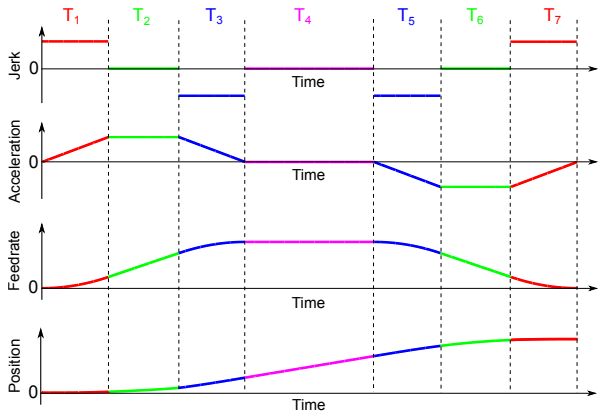

Fig. 1 Kinematic profiles for trapezoidal acceleration

The main idea of the paper consists in obtaining the highest tangential jerk and acceleration values on the tool path in order to reduce machining time. To reach this objective, the tool orientation can be managed along the tool path. So the aim is to find the tool orientation strategy in 3+2-axis machining to generate the highest kinematics of the tool with respect to the

part. Thus it is necessary to establish the relationship between kinematics of all axes in the joint space and kinematics at the tool tip in the part space.

2.3 Forward and inverse kinematics

By noting $\mathbf{q}$ the axis position, the end-effector position and orientation in the part space is noted $\mathbf{X}$. Forward kinematics allows linking the velocity evolution of the end-effector $\dot{\mathbf{X}}$ in the part space with the velocity evolution $\dot{\mathbf{q}}$ in the joint space thanks to the Jacobian matrix $\mathbf{J}(\mathbf{q})$ (Equation 2). This is the first order kinematic model.

$$\dot{\mathbf{X}} = \mathbf{J}(\mathbf{q}).\dot{\mathbf{q}} \quad \text{with} \quad \mathbf{J}(\mathbf{q}) = \frac{\partial \mathbf{X}}{\partial \mathbf{q}} \tag{2}$$

The second and third order kinematic models link respectively the joint acceleration to the acceleration in the part space and the joint jerk to the jerk in the part space. Equations 3 and 4 are obtained by deriving Equation 2.

$$\ddot{\mathbf{X}} = \mathbf{J}(\mathbf{q}).\ddot{\mathbf{q}} + \dot{\mathbf{J}}(\mathbf{q},\dot{\mathbf{q}}).\dot{\mathbf{q}} \tag{3}$$

$$\dddot{\mathbf{X}} = \mathbf{J}(\mathbf{q}).\dddot{\mathbf{q}} + 2.\dot{\mathbf{J}}(\mathbf{q},\dot{\mathbf{q}}).\ddot{\mathbf{q}} + \ddot{\mathbf{J}}(\mathbf{q},\dot{\mathbf{q}},\ddot{\mathbf{q}}).\dot{\mathbf{q}} \tag{4}$$

In the general case, relative feedrate, acceleration and jerk characterize performances of the tool path execution. The end-effector velocity, acceleration and jerk are expressed with three coordinates in the part space $(\dot{X}_p,\dot{Y}_p,\dot{Z}_p)$, $(\ddot{X}_p,\ddot{Y}_p,\ddot{Z}_p)$, $(\dddot{X}_p,\dddot{Y}_p,\dddot{Z}_p)$.

The interest of such an approach with polytopes is to fully characterize geometrically these capacities and to easily determine the position and orientation that maximize them. Section 3 specifies manipulability polytope and its use to define an optimized workpiece setup.

3 Kinematic manipulability

3.1 Kinematic limits modelling

Yoshikawa was the first to model kinematic capacities by introducing manipulability ellipsoids [27]. These ellipsoids correspond to the kinematic limits of each axis in the joint space. This model is often used for its quadratic expression easy to manipulate in the part space with the use of the Jacobian matrix $\mathbf{J}$. Different kinematic performance indices based on $\mathbf{J}$ can be considered, such as singular values, condition number, dexterity, etc.

However such a model and associated parameters lead to an underestimation of the real capacities. Joint kinematic limits are initially modelled by a unit sphere (considering normalizing), i.e., for the velocity $\|\dot{\mathbf{q}}\| = 1$. With this hypothesis, the Euclidean norm links the maximum or minimum values of the axes.

Considering the machine tool technological point of view, each machine axis q_i has its own kinematic limits based on actuator, transmission and machine architecture. Hence, the kinematic limits of the axes in the joint space are independent of each other. Thus, kinematic performances are no longer modelled by ellipsoids but by a unit cube (considering normalizing). This model, named polytope, represents in a relevant way the joint capacities.

Thus, maximum velocity, acceleration and jerk limits are represented as polytopes in the joint space of the machine tool. One can see on Figure 2 that joint polytopes include the manipulability ellipsoid, and thus are more suited to express actual machine performances [28, 29].

Thanks to the Jacobian matrix and its derivatives (Equations 2 to 4), it is also possible to obtain kinematic limits in the part space.

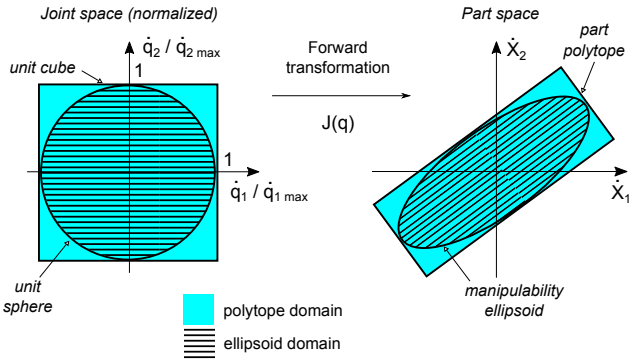

Fig. 2 Different modelling of the kinematic axes performances

3.2 Mathematical definition of polytopes

A polytope is a bounded polyhedron composed of polygonal flat faces. A polytope can be described either as a V-description (vertices description) or as a H-description (Half-space description). In a V-description, a m dimensional (mD) polytope is defined as a convex hull of a set of points V_i in $\mathbb{R}^n$ with $m \leqslant n$ and V_i the polytope vertices [30]. In a H-description, a polytope is the bounded intersection of a finite set of closed half-spaces of which the boundaries are hyperplanes [31]. A mD polytope can be defined by a system of inequalities composed by enclosed half-spaces (Equation 5).

$$P = P(\mathbf{A},\mathbf{b}) = \mathbf{x} \in \mathbb{R}^n : \mathbf{A}.\mathbf{x} \leqslant \mathbf{b} \tag{5}$$

with $\mathbf{A} \in \mathbb{R}^{m \times n}$ and $\mathbf{b} \in \mathbb{R}^m$.

Figure 3 shows the same 2D polytope in $(\mathbf{x}_1,\mathbf{x}_2)$ either with a H-description or with a V-description.

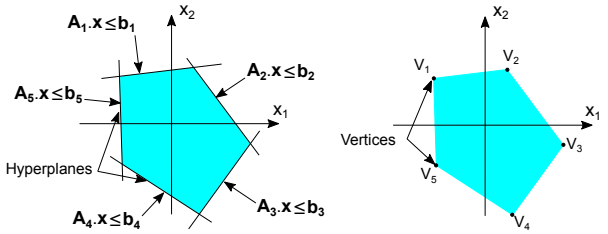

Fig. 3 H-description and V-description for a 2D polytope

Table 1 Kinematic characteristics of the Mikron UCP 710 machine

	X_m	Y_m	Z_m	A	C
$V^{\max}$ $(\mathrm{m.s}^{-1}, \mathrm{rev.s}^{-1})$	0.5	0.5	0.5	0.25	0.33
$A^{\max}$ $(\mathrm{m.s}^{-2}, \mathrm{rev.s}^{-2})$	2.5	3	2.1	0.83	0.83
$J^{\max}$ $(\mathrm{m.s}^{-3}, \mathrm{rev.s}^{-3})$	5	5	5	5	50

3.3 Application to machine tools

To illustrate developments throughout the rest of the paper, polytope representations are given for the 5-axis machine tool Mikron UCP 710 whose structure is $V\,[w\,C'\,A'\,b\,X_m\,Y_m\,Z_m\,(C1)\,t]$ according to the ISO10791 standard. Nevertheless, the proposed method can be applied to any other poly articulated structures. For the Mikron machine, kinematic limits of each axis are given in Table 1.

3.3.1 Joint polytopes

To obtain a graphical representation of these 5D polytopes (5-axis machine tool), they must be projected into one or several 3D spaces. Figure 4 shows maximal velocity hyperplanes for the 3 linear axes X_m, Y_m and Z_m and for the rotary axes A and C combined with Z_m. Intersections of hyperplanes give edges and vertices of the velocity polytope. The shape of linear axes velocity polytope is a cube because velocity limits of each linear axis are the same (0.5 $\mathrm{m.s}^{-1}$). For rotary axes, units are converted from $\mathrm{rev.s}^{-1}$ to $\mathrm{rad.s}^{-1}$.

3.3.2 Transformation from joint space to part space

The tool path is expressed in the part space with six components: three for the tool tip location and three for the cosines of the tool axis orientation (X_p,Y_p,Z_p,i,j,k). Based on the first order kinematic model (Equation 2), switching from the joint space to the part space is a linear application for a given axes configuration. Thus, a 5D velocity polytope in the joint space gives a 6D velocity polytope in the part space.

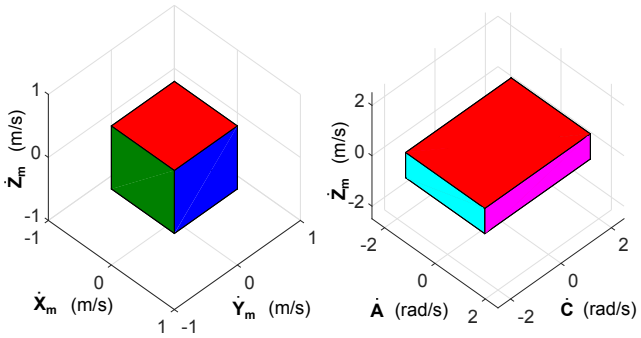

Fig. 4 5D joint velocity polytope projected in two 3D spaces for visualization

Figure 5 shows the impact of the rotary axes A and C on a 5-axis positioned machining. The shape of the velocity polytope is the same but its orientation changes in the part space. Rotary axes do not change the polytope geometry in projection on linear axes.

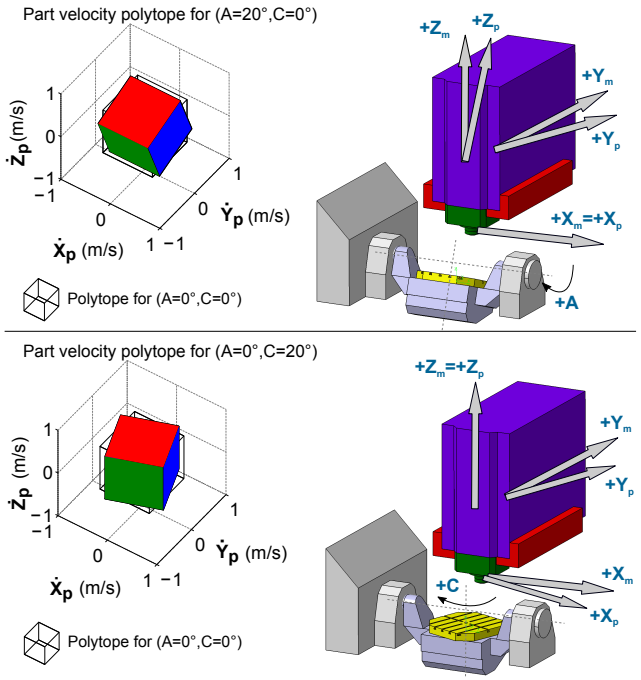

Fig. 5 Influence of A and C axes on velocity polytope in the part space in 3+2-axis machining

4 Principles of tool orientation optimization

The aim is to determine the tool orientation (i.e. rotary axes values A^{sol} and C^{sol}) for each tool path or for the whole part in order to have maximum tangential velocity, acceleration and jerk in the part space.

4.1 Maximum norm directions

Equations 6 give the Euclidean norm in the joint space for each kinematic level based on the characteristics of the three linear axes in 3+2-axis machining, with a serial architecture machine tool. They represent the kinematic composition of machine axes.

$$\begin{cases} \|\dot{\mathbf{q}}\| = \sqrt{\sum_{i\in[\![1\,;3]\!]} \dot{q}_i{}^2} \\ \|\ddot{\mathbf{q}}\| = \sqrt{\sum_{i\in[\![1\,;3]\!]} \ddot{q}_i{}^2} \\ \|\dddot{\mathbf{q}}\| = \sqrt{\sum_{i\in[\![1\,;3]\!]} \dddot{q}_i{}^2} \end{cases} \tag{6}$$

In the joint space, vectors $\dot{\mathbf{q}}$, $\ddot{\mathbf{q}}$, and $\dddot{\mathbf{q}}$, are oriented by a unit direction $\mathbf{d}$. For a given unit direction $\mathbf{d}$ defined in the joint space corresponds the feedrate direction $\mathbf{f}$ in the part space. All possible directions of $\dot{\mathbf{q}}$, $\ddot{\mathbf{q}}$, and $\dddot{\mathbf{q}}$ can be illustrated by a sphere (Figure 6). A particular direction can be represented by a vector starting from the origin and whose extremity reaches the corresponding polytope (face, edge or vertex). Hence, the eight maximum norm values correspond to the eight polytope vertices. In such a configuration, directions are called preferred directions and noted $\mathbf{d}_{\text{vel.}}$, $\mathbf{d}_{\text{acc.}}$ or $\mathbf{d}_{\text{jerk}}$.

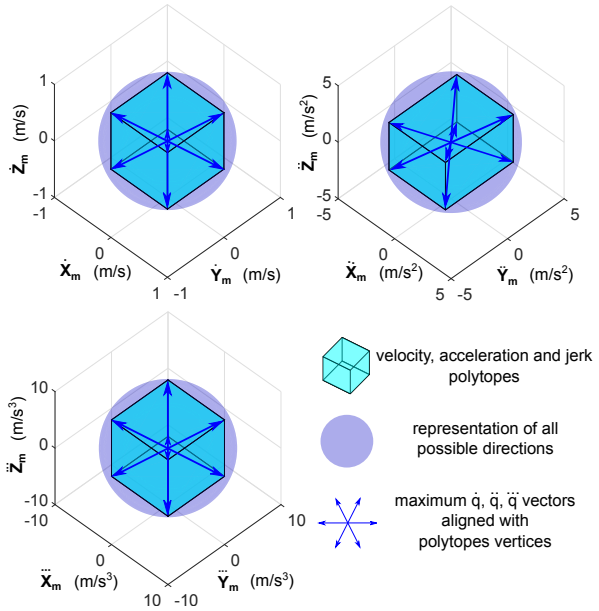

Fig. 6 Maximum norm directions for the different kinematic levels

Table 2 illustrates that the preferred directions and the corresponding maximum norms for the three kinematic levels (velocity, acceleration, jerk) are not the same because of the different distribution of axis kinematics (Table 1). Indeed, maximum axis jerk is the same for the X_m,Y_m and Z_m axis (5 m.s^{-3}) but for maximum acceleration Y_m axis is 3 m.s^{-2} whereas X_m and Z_m axes are 2.5 and 2.1 m.s^{-2}.

Table 2 Maximum kinematic levels functions of directions

preferred directions	$\|\dot{\mathbf{q}}(\mathbf{d})\|$ (m.s^{-1})	$\|\ddot{\mathbf{q}}(\mathbf{d})\|$ (m.s^{-2})	$\|\dddot{\mathbf{q}}(\mathbf{d})\|$ (m.s^{-3})
$\mathbf{d}_{\text{vel.}}$	**0.87**	3.6	8.7
$\mathbf{d}_{\text{acc.}}$	0.74	**4.4**	7.4
$\mathbf{d}_{\text{jerk}}$	0.87	3.6	**8.7**

Thus, it is not possible to choose an orientation which simultaneously maximizes velocity, acceleration and jerk. It is necessary to find which direction in the joint space, or which parameter among velocity, acceleration and jerk has the most influence on the actual feedrate and on the total machining time.

4.2 Limiting parameter determination

In a jerk controlled movement law, the first saturation happens in jerk and then maybe in acceleration or in velocity according to kinematic levels and tool path geometry. Thus, jerk level should be taken into account as well as acceleration and velocity. Figure 6 shows that velocity, acceleration and jerk norms depend on the direction $\mathbf{d}$, namely the ratio of axes solicitations. Maximal reachable available velocity, acceleration and jerk norm is defined by the intersection between the direction $\mathbf{d}$ and the corresponding polytope boundary (Equation 7).

$$\begin{cases} \|\dot{\mathbf{q}}(\mathbf{d})\| = \min\limits_{i\in[\![1\,;3]\!]} \left| \dfrac{\dot{q}_{\text{i}}{}^{\max}}{d_i} \right| \\ \|\ddot{\mathbf{q}}(\mathbf{d})\| = \min\limits_{i\in[\![1\,;3]\!]} \left| \dfrac{\ddot{q}_{\text{i}}{}^{\max}}{d_i} \right| \\ \|\dddot{\mathbf{q}}(\mathbf{d})\| = \min\limits_{i\in[\![1\,;3]\!]} \left| \dfrac{\dddot{q}_{\text{i}}{}^{\max}}{d_i} \right| \end{cases} \tag{7}$$

Thus, within the context of 3+2-axis machining, it would be interesting to find a direction which optimally combines kinematic levels that is to say maximum jerk, maximum acceleration and maximum velocity capacities. When considering a given tool path with both jerk and acceleration saturation during execution, the optimal direction is necessarily between the maximum jerk direction and the maximum acceleration direction. An example of such a configuration is given in Figure 7.

The intersections between polytopes and the potential optimal directions give corresponding maximum jerk and acceleration values. If the candidate optimal

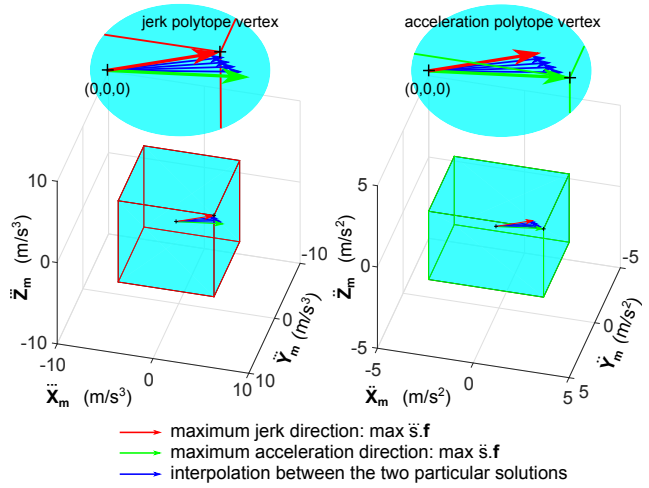

Fig. 7 Possible optimal orientation directions

direction changes from the preferred jerk direction to the preferred acceleration direction, the maximal jerk value decreases whereas the maximal acceleration value increases. Thanks to these kinematic levels and the jerk movement law, it is possible to estimate machining time. Then, given a local straight line path and its corresponding joint direction, the maximum jerk and acceleration values enable with the jerk controlled law movement to determine the machining time.

4.3 Influence of jerk limits on the actual feedrate

Machining time is given by the evolution of the actual feedrate $\dot{s}$ along the path (Equation 8) where s is the abscissa and L the total length.

$$t_{\text{machining}} = \int_0^L \frac{1}{\dot{s}}\, ds \tag{8}$$

Once transformed in the part space, polytope graphically represents the maximum norm in the local feed direction $\mathbf{f}$ of the tool path. The feedrate $\dot{\mathbf{X}}$ is a function of the feed direction $\mathbf{f}$ and the tangential velocity $\dot{s}$. Acceleration $\ddot{\mathbf{X}}$ and jerk $\dddot{\mathbf{X}}$ in the part space are functions of the feed direction, its first and second derivatives. Equation 9 gives the decomposition for the three kinematic levels where the feed direction and its derivatives are functions of the tool path geometry $\mathbf{X}$ (Equation 10).

$$\begin{cases} \dot{\mathbf{X}} = \dot{s}.\mathbf{f} \\ \ddot{\mathbf{X}} = \ddot{s}.\mathbf{f} + \dot{s}^2.\dfrac{d\mathbf{f}}{ds} \\ \dddot{\mathbf{X}} = \dddot{s}.\mathbf{f} + 3\,\ddot{s}.\dot{s}.\dfrac{d\mathbf{f}}{ds} + \dot{s}^3.\dfrac{d^2\mathbf{f}}{ds^2} \end{cases} \tag{9}$$

$$\begin{cases} \mathbf{f} = \dfrac{d\mathbf{X}}{ds} \\ \dfrac{d\mathbf{f}}{ds} = \dfrac{d^2\mathbf{X}}{ds^2} \\ \dfrac{d^2\mathbf{f}}{ds^2} = \dfrac{d^3\mathbf{X}}{ds^3} \end{cases} \tag{10}$$

When the tool path is a perfect straight line, the tangential vector $\mathbf{f}$ is constant along the path displacement. Nevertheless, its derivatives are null. But this is not the case for complex tool paths and freeform surfaces. Focusing on "stretched" surfaces, derivative terms of $\mathbf{f}$ are assumed to be negligible compared to feed direction term $\mathbf{f}$, leading to Equation 11.

$$\begin{cases} \dot{\mathbf{X}} = \dot{s}.\mathbf{f} \\ \ddot{\mathbf{X}} = \ddot{s}.\mathbf{f} \\ \dddot{\mathbf{X}} = \dddot{s}.\mathbf{f} \end{cases} \tag{11}$$

As previously discussed in section 4, tangential jerk $\dddot{s}$ is the most relevant parameter during the execution of the tool path especially in high speed machining. As a consequence, in order to find the optimal orientation, it is necessary to solve Equation 12 while maximizing $\dddot{s}$.

$$\dddot{s}.\mathbf{f} = \mathbf{J}(\mathbf{q}).\ddot{\mathbf{q}} \tag{12}$$

For a feed direction $\mathbf{f}_{\text{path}}$ representative of the given tool path, the aim is to find rotary axes values, i.e., the components A^{sol} and C^{sol} of $\mathbf{q}$, which provide maximum tangential jerk in the part space.

$$\left\{A^{\text{sol}}, C^{\text{sol}}\right\} = \arg \max_{\{A,C,\ddot{\mathbf{q}}\}} \|\mathbf{J}\,(A,C)\,.\ddot{\mathbf{q}}\| \tag{13}$$

submitted to constraint

$$\dddot{s}.\mathbf{f}_{\text{path}} = \mathbf{J}(A^{\text{sol}}, C^{\text{sol}}).\ddot{\mathbf{q}} \tag{14}$$

The upper limit of the maximum tangential jerk ($\max \dddot{s}$) is reached when $\mathbf{f}_{\text{path}}$ can be aligned with a vertex:

$$\max \|\dddot{s}.\mathbf{f}_{\text{path}}\| \leqslant \|\mathbf{J}\left(A^{\text{sol}}, C^{\text{sol}}\right).\ddot{\mathbf{q}}_{\text{vertex}}\| \tag{15}$$

For a machine tool structure with rotary and tilting table such as the Mikron UCP 710 machine, the Jacobian matrix has the following expression (Equation 16):

$$\mathbf{J}(A,C) = \begin{bmatrix} \cos C & -\cos A \sin C & \sin A \sin C \\ \sin C & \cos A \cos C & -\sin A \cos C \\ 0 & \sin A & \cos A \end{bmatrix} \tag{16}$$

In 3+2-axis machining, $\mathbf{J}(A,C)$ represents a rotation matrix. Thus, it preserves the norm of the vectors:

$$\mathbf{f}_{\text{path}} = \mathbf{J}(A,C).\frac{\ddot{\mathbf{q}}}{\|\ddot{\mathbf{q}}\|} \tag{17}$$

When $\mathbf{f}_{\text{path}}$ can be aligned with a vertex, Equation 17 is rewritten:

$$\mathbf{f}_{\text{path}} = \mathbf{J}(A^{\text{sol}}, C^{\text{sol}}).\frac{\ddot{\mathbf{q}}_{\text{vertex}}}{\|\ddot{\mathbf{q}}_{\text{vertex}}\|} \tag{18}$$

with

$$\max \ddot{s} = \|\ddot{\mathbf{q}}_{\text{vertex}}\| \tag{19}$$

Such a problem has 16 solutions $\{A^{\text{sol}}, C^{\text{sol}}\}$: 2 solutions $\{A^{\text{sol}}, C^{\text{sol}}\}$ corresponding to each of the 8 possible vertices $\ddot{\mathbf{q}}_{\text{vertex}}$ of the joint polytope. Method for solving explicit solutions $\{A^{\text{sol}}, C^{\text{sol}}\}$ of Equation 18 is detailed in A.

A first example is given on Figure 8. It represents the particular case where the part space is identical to the joint space. In this trivial case, when $\mathbf{f}_{\text{path 1}} = \frac{1}{\sqrt{3}}[1,1,1]^{\intercal}$ in the part space, the feed direction is natively aligned with the vertex $\ddot{\mathbf{q}}_{\text{vertex}} = \left[\ddot{q}_{X_m}^{\max}, \ddot{q}_{Y_m}^{\max}, \ddot{q}_{Z_m}^{\max}\right]^{\intercal}$. Hence, the first obvious solution is $\left\{A_1^{\text{sol}} = 0°, C_1^{\text{sol}} = 0°\right\}$. Nevertheless one can see that a second solution $\left\{A_2^{\text{sol}} = 90°, C_2^{\text{sol}} = 90°\right\}$ exists and is also aligned with the same vertex.

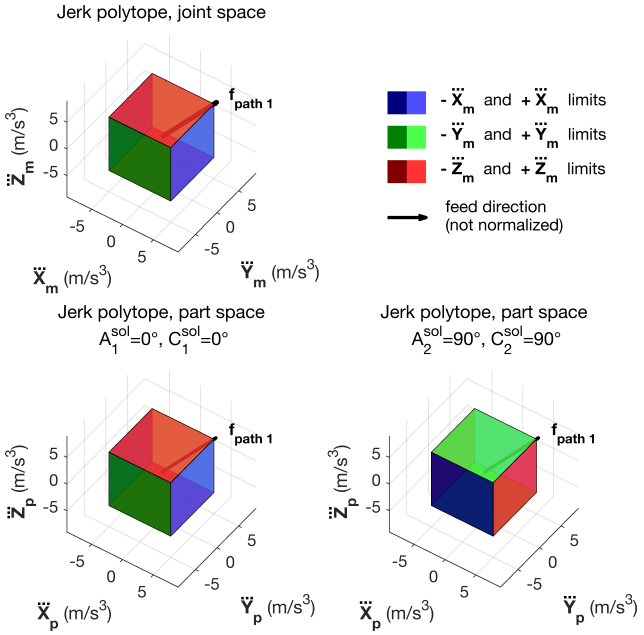

Fig. 8 $\{A^{\text{sol}}, C^{\text{sol}}\}$ solutions for $\mathbf{f}_{\text{path 1}} = \frac{1}{\sqrt{3}}[1,1,1]^{\intercal}$

A second example represented in Figure 9 is the case where $\mathbf{f}_{\text{path 2}} = [1,0,0]^{\intercal}$ in the part space and where the vertex $\ddot{\mathbf{q}}_{\text{vertex}} = \left[\ddot{q}_{X_m}^{\min}, \ddot{q}_{Y_m}^{\min}, \ddot{q}_{Z_m}^{\max}\right]^{\intercal}$ is pointed. One can see on the figure the two corresponding solutions, where the polytope is rotated in the part space.

However, the feed direction can't always be aligned with a vertex. Intrinsic rotations of the part performed by the rotary axes of the machine dot not permit to orientate the part as desired in the joint space. This

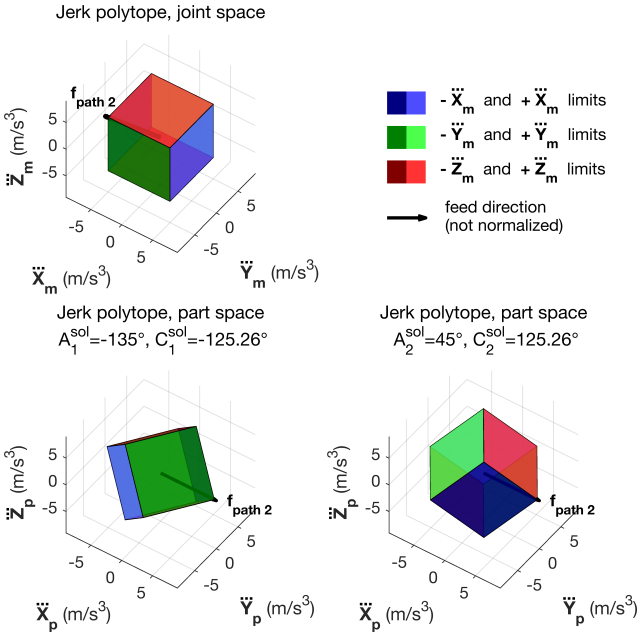

Fig. 9 $\{A^{\text{sol}}, C^{\text{sol}}\}$ solutions for $\mathbf{f}_{\text{path 2}} = [1,0,0]^{\intercal}$

condition is depending on the machine architecture and on the geometry of the considered joint polytope.
This can also be retrieved while solving Equation 28, where the condition for the existence of solutions is as follows for the Mikron machine:

$$\ddot{q}_{\text{y vertex}}{}^2 + \ddot{q}_{\text{z vertex}}{}^2 \geqslant \|\ddot{\mathbf{q}}_{\text{vertex}}\|^2 \, f_z{}^2 \tag{20}$$

Figure 10 shows all the possible orientations of the feed direction in the part space as a unit sphere. If the component of $\mathbf{f}_{\text{path}}$ along the Z-axis is too high, i.e., the feed direction is too vertical, there is no solution for $\{A^{\text{sol}}, C^{\text{sol}}\}$; since Equation 20 cannot be satisfied, the part can't be oriented such as $\mathbf{f}_{\text{path}}$ is aligned with a vertex. Hence two areas of non-existence of solutions are present at the poles of the unit sphere (blue regions).

When a vertex cannot be reached, a solution of Equation 13 is obtained when $\ddot{\mathbf{q}}$ raises along the edges of the polytope towards a vertex. As a consequence, the maximal value of the tangential jerk $\ddot{s}$ decreases from the vertex distance to the origin $\|\ddot{\mathbf{q}}_{\text{vertex}}\|$ (considering normalizing $= \sqrt{3}$ or the diagonal of the unit cube) to a minimum value that is the distance of the polytope edges to the origin (considering normalizing $= \sqrt{2}$).
Let set $\mathbf{f}_{\text{path 3}} = [0,0,1]^{\intercal}$ in the part space. Equation 20 is not satisfied whichever vertex is chosen. Figure 11 shows two particular solutions that correspond to its better alignment with $\ddot{\mathbf{q}}_{\text{vertex}} = \left[\ddot{q}_{X_m}^{\max}, \ddot{q}_{Y_m}^{\max}, \ddot{q}_{Z_m}^{\max}\right]^{\intercal}$. In this particular case, there's an infinite number of solutions: $A^{\text{sol}} = 45°$ and C^{sol} is undetermined. Hence, these solutions of Equation 13 maximize the tangential jerk.
One can see on Figure 12 that the maximum tangen-

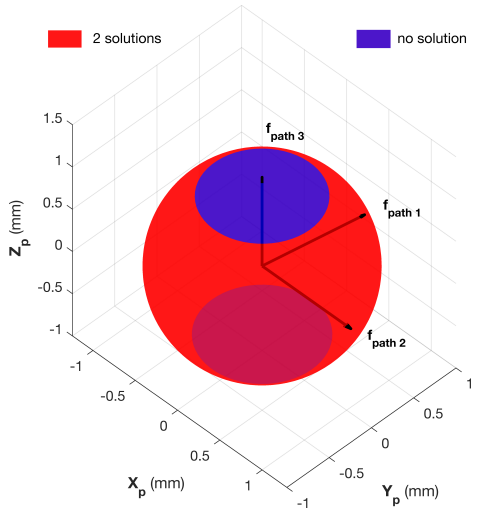

Fig. 10 Existence of solution $\{A^{\text{sol}}, C^{\text{sol}}\}$ to align feed direction to a vertex

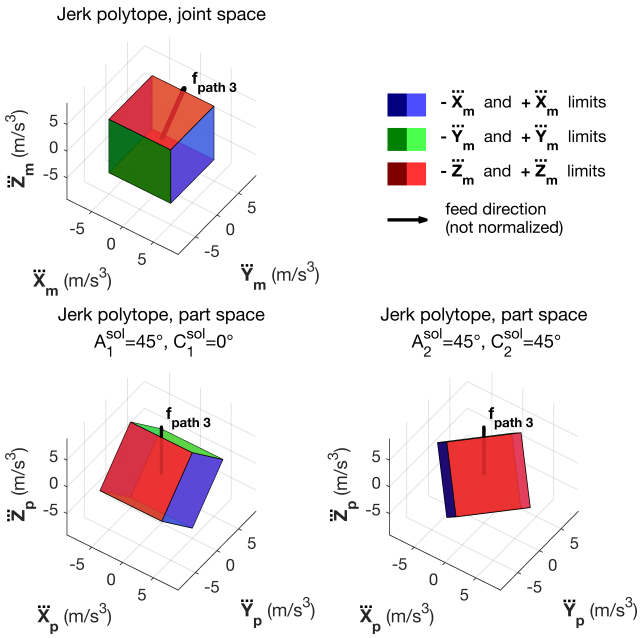

Fig. 11 $\{A^{\text{sol}}, C^{\text{sol}}\}$ solution for $\mathbf{f}_{\text{path 3}} = [0, 0, 1]^{\intercal}$

tial jerk is depending on the feed direction in the part space. For the Mikron machine, it is equal to $5\sqrt{3}$ m.s^{-3} (approximately 8.7 m.s^{-3}) over a large portion of the unit sphere. This is the case for $\mathbf{f}_{\text{path 1}}$ and $\mathbf{f}_{\text{path 2}}$. At the poles, the maximum value decreases to $5\sqrt{2}$ m.s^{-3} (approximately 7.1 m.s^{-3}), which is the case for $\mathbf{f}_{\text{path 3}}$.

With a AC rotary axes machine, the highest value of the maximum tangential jerk that can be reached corresponds to the diagonal of the jerk polytope, and its minimum value corresponds to the distance to the edges based on Y_m and Z_m axes to the origin:

$$\sqrt{J_{Y_m}^{\max 2} + J_{Z_m}^{\max 2}} \leqslant \max \dddot{s} \leqslant \sqrt{J_{X_m}^{\max 2} + J_{Y_m}^{\max 2} + J_{Z_m}^{\max 2}} \quad (21)$$

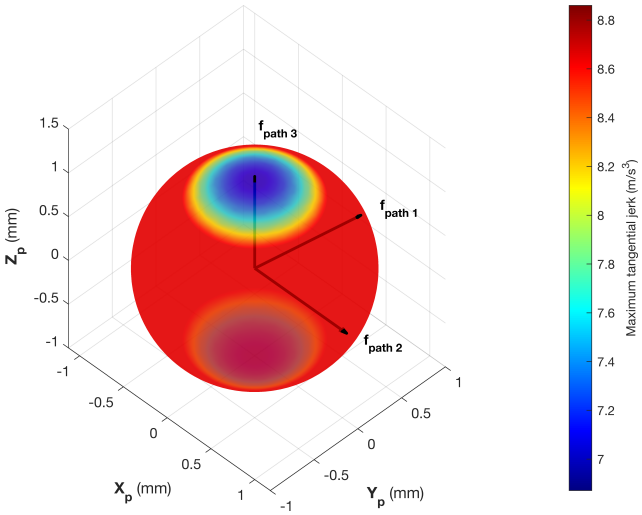

Fig. 12 Maximal value of tangential jerk function of feed direction

In conclusion, without loss of generality for other serial architectures of 5-axis machines, the maximum reachable tangential jerk can easily be bounded based on jerk axes performances. In any case, the tangential jerk gain is important compared to the use of the machine axes separately.

$$\min\left(J_{X_m}^{\max}, J_{Y_m}^{\max}, J_{Z_m}^{\max}\right) \ll \max \dddot{s} \quad (22)$$

4.4 Additional constraints

Among these multiple theoretical solutions, additional constraints such as axis ranges, accessibility, non-collision, admissible cutting conditions should be taken into account to evaluate the most appropriated one.

As rotary axes are fixed within a path in 3+2 machining, it is necessary to check that at least one solution exists for the inverse kinematics, especially for rotary axes because of their limited ranges. In order to machine with feasible cutting conditions, it is possible to limit the domain of admissible tool axis orientation. For that purpose, tilt and yaw angles from the unit normal vector $\mathbf{n}$ can be chosen. For example, considering a parameterization of the tool axis orientation with the angle θ_f around the feed vector $\mathbf{f}$ and the angle θ_t around the unit transverse vector $\mathbf{t}$ (based on the local frame ($\mathbf{f}$,$\mathbf{n}$,$\mathbf{t}$) of the tool path), the Figure 13 illustrates the domain of admissible orientation defined by a pyramid. Moreover, as $\mathbf{n}$ and $\mathbf{f}$ may vary along the tool path and given that the rotary axes values are fixed for the whole part or on one path, the angles θ_f and θ_t may also vary. A feasible solution regarding the cutting conditions should also be included in the domain of admissible orientation.

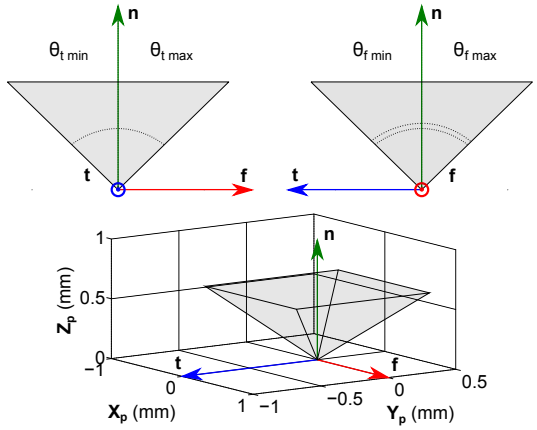

Fig. 13 Domain of admissible orientation

Experimental applications are realized in the next section to show the efficiency and the limits of the proposed method. One test part is a hyperbolic paraboloid surface which allows machining straight lines and the second one is a "stretched" surface extracted from literature.

5 Experimental applications in 3+2-axis machining

5.1 Test part 1: hyperbolic paraboloid

The first chosen surface is quite a small one (100 mm × 100 mm), based on a hyperbolic paraboloid whose control points are given in B. Rules (straight line generatrix) are oriented at 45 degrees to X_p and Y_p axes and allow to generate 3+2-axis tool paths (Figure 14). In this example, the surface represents directly the locus of the tool center point that is chosen to be the center of the sphere for the ball end mill. In such a way, the machined surface is independent of the tool axis orientation.

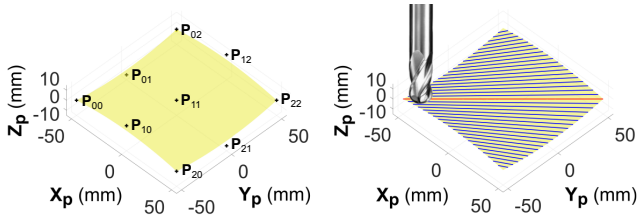

Fig. 14 Test part n°1: hyperbolic paraboloid

The milling strategy is based on a parallel plans sweeping mode according to paraboloid rules such as the cutter location path is made of one linear segment for each path. For the different experiments, the selected tool is a solid carbide 16 mm diameter ball end mill with four teeth. The diameter of the tool is large enough to have a high number of teeth. However, it remains compatible with the curvatures of the surface. Thanks to this, the feedrate of the tool can be very high, which illustrates the kinematic optimization sought in this article. The cutting conditions are thus chosen towards the upper limits of the intervals recommended by the tool manufacturer. Within the context of copying freeform surfaces in High Speed Machining, cutting parameters for 7000 series aluminium are a feed per tooth equal to 0.3 mm and a cutting speed equal to 1200 m.min^{-1}. Hence with a 24000 rpm spindle, the programmed feedrate is equal to 30 m.min^{-1}.
The part is classically set up on the machine table such as the part frame (X_p,Y_p,Z_p) corresponds to the axis machine frame (X_m,Y_m,Z_m) with $A = C = 0$. To let a maximum of degrees of freedom for the optimization, tool axis orientation is allowed to change between each path. Thus, configuration is 3+2 -axis machining. It is possible to freely change the orientation without risk of collisions up to good cutting conditions as mentioned in section 4.4.

5.1.1 Kinematic optimization

Using the proposed method, it is possible to find A and C values that maximize the use of kinematics considering the jerk polytope. A^{sol} and C^{sol} make the jerk polytope rotate in the part space such that the feed direction vector $\mathbf{f}_{\text{path}}$ is aligned towards one of the polytope vertices. In such a configuration, tangential jerk $\dddot{s}$ is maximum, equal to 8.7 m.s^{-3}, and makes full use of the machine capacities. Figure 15 shows the solution orientation for each path. Path number 1 is located close to the P_{02} control point of the surface. A^{sol} solutions vary from 50 to 15 degrees and C^{sol} solutions are about 10.8 degrees.

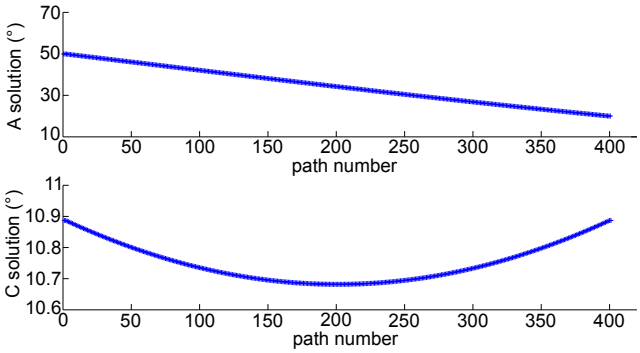

Fig. 15 A and C solutions for each path

5.1.2 Experimental validation

Tests are carried out on the Mikron UCP 710 machine and axes velocities are recorded throughout the CNC during the tool path execution. Figure 16 highlights the difference of behaviour of the actual feedrate. It compares the initial orientation where A and C are both null (default orientation) with the one given by the jerk polytope that maximizes the tangential jerk norm in the part space.

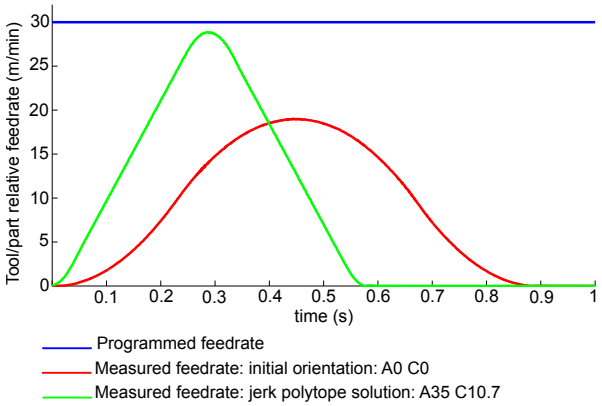

Fig. 16 Measured relative feedrates for path n°200 with different (A,C) orientations

Considering the example of path n°200, the maximal reached feedrate is 40% higher and thus, machining time is reduced by about 45%. This simple example shows the efficiency of the orientation optimization considering machine kinematics.
However, the principle of optimization for each path of the trajectory has a major disadvantage: as the geometry evolves from one path to another, the optimal (A,C) orientations are slightly different for each path. Therefore, during execution, the machine has to move the rotary axes very slightly between two successive paths, which takes time. Optimizing the orientation independently per path does not result in the shortest possible machining time for the entire workpiece.

In order to overcome this problem, within the context of stretched surfaces, it is possible to no longer consider the solution orientation per path, but the optimal orientation for all the trajectory. The optimal $(A^{\text{opt}}_{\text{part}},C^{\text{opt}}_{\text{part}})$ solution for the part can be defined as the average $\mathbf{f}^{\text{opt}}_{\text{part}}$ of the feed directions per path $\mathbf{f}^{\text{sol}}_{\text{path i}}$, weighted by the length of each path $\Delta s_{\text{path i}}$ (Equation 23).

$$\mathbf{f}^{\text{opt}}_{\text{part}} = \frac{\sum_i \mathbf{f}^{\text{sol}}_{\text{path i}}\,\Delta s_{\text{path i}}}{\sum_i \Delta s_{\text{path i}}} \quad i \in [\![1;\text{number of paths}]\!] \tag{23}$$

Thus, the corresponding solution $(A^{\text{opt}}_{\text{part}},C^{\text{opt}}_{\text{part}})$ retained is close to all the solutions $(A^{\text{sol}}_{\text{path i}},C^{\text{sol}}_{\text{path i}})$ corresponding to each path i.

Table 3 summarizes recorded total machining time for different optimization strategies. These values confirm that for small sized parts, the optimal jerk polytope orientation is reached considering the whole part and the mean of the feed direction for all paths.

Table 3 Measured total machining times for different optimization strategies

Strategies	Machining time	Time saving
Basic orientation $(A=0,C=0)$	5 min 17 s	–
Jerk polytope solution by path $(A^{\text{sol}}_{\text{path i}},C^{\text{sol}}_{\text{path i}})$	4 min 23 s	17%
Jerk polytope optimization whole part $(A^{\text{opt}}_{\text{part}},C^{\text{opt}}_{\text{part}})$	3 min 39 s	31%

However, care must be taken during the execution of the trajectory that the maximization of the feedrate is not to the detriment of the quality of the machined surface by potential vibrations that could appear. It is important to keep in mind that the dynamic behaviour of the axes must be adjusted and contained by the maximum jerk level. Furthermore, in order to guarantee a certain cutting regularity and possible high fluctuations, a jerk parameter, tangent to the trajectory, can be defined and set to prevent the cutting conditions of the tool from varying too strongly locally and thus degrading the quality of the machined surface. In general, the balance between kinematics and cutting stability must be maintained.

5.2 Test part 2: Manta surface

This second test part is larger (600 mm × 600 mm) and is inspired from bibliography. It was previously studied for setup optimization by Pessoles et al. [16]. Figure 17 shows the nominal part which presents variations of the surface normal. Surface geometry has a double curvature such as tool paths are not linear segments but BSpline curves. Surface definition is given in C.

The milling strategy is based on parallel planes sweeping mode according to Y-axis and the workpiece setup is parallel to machine tool axes. A ball-end tool of 16 mm diameter is also used in this example. The aim of this

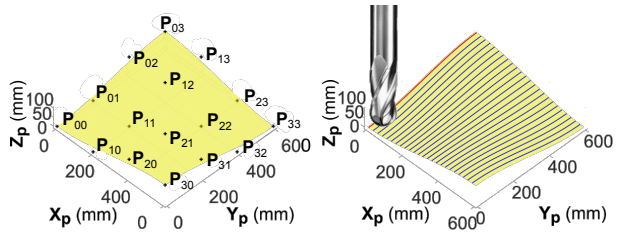

Fig. 17 Test part n°2: Manta surface

section is to find the optimal A and C values for each path ($A^{\text{sol}}_{\text{path i}}$,$C^{\text{sol}}_{\text{path i}}$) assuming that tool axis orientation is allowed to change between each path, and the solution for the whole machining ($A^{\text{opt}}_{\text{part}}$,$C^{\text{opt}}_{\text{part}}$).

5.2.1 Kinematic optimization

As each path of the surface is a complex curve and no longer a linear segment, it is necessary to find A and C orientations which allow aligning one of the jerk polytope vertices in the mean feed direction $\mathbf{f}^{\text{mean}}_{\text{path i}}$ of each path i. The retained feed direction for a path is based on the weighted average along the curvilinear abscissa (Equation 24).

$$\mathbf{f}^{\text{mean}}_{\text{path i}} = \frac{1}{s_i} \int_0^{s_i} \mathbf{f}(s).ds \tag{24}$$

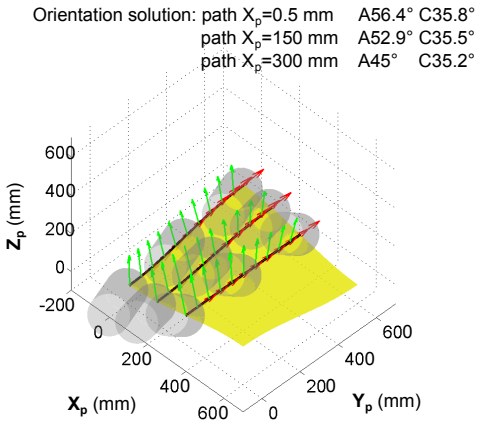

Fig. 18 Tool axis orientation solution for the three paths

Figure 18 shows tool orientation solutions for three paths ($X_p = 0.5$ mm, $X_p = 150$ mm and $X_p = 300$ mm). As expected, the solution orientation is different for each path and changes progressively. Besides, the feed direction does not match exactly along the whole path to one of the polytope vertices but the mean feed direction is aligned with the jerk polytope vertex (Figure 19).

Thus, time saving during tool path execution would be less important when there are more feed direction

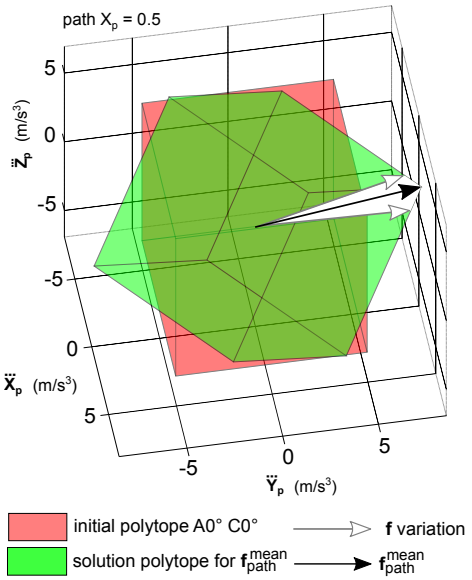

Fig. 19 **f** variation and resulting mean for a path

variations along a path. To illustrate this point, next section investigates experiments on the Mikron UCP 710 machine to compare the three studied paths.

5.2.2 Experimental validation

Figure 20 shows that machining time is reduced for the three paths, but as could be expected, the time saving is not the same. Indeed, the geometry of the path and thus the variation of the feed direction, changes with the path location on the part. For paths close to the edge of the workpiece, the curvatures and variations in curvature are slightly higher. Thus, the most complex path is path $X_p = 0.5$ mm and the most straight path is path $X_p = 300$ mm. Since the optimal orientation ($A^{\text{sol}}_{\text{path i}}$,$C^{\text{sol}}_{\text{path i}}$) for each path is chosen according to the $\mathbf{f}^{\text{mean}}_{\text{path i}}$ criterion, the more straight path is, the closer the solution ($A^{\text{sol}}_{\text{path i}}$,$C^{\text{sol}}_{\text{path i}}$) is to all local orientations of the local feed vector $\mathbf{f}(s)$. The kinematic gain is thus even more important. For the three selected paths, the time saving varies from 13% to 38%.

As previously mentioned, it is always possible to determine the overall optimal orientation for the machining of the whole part and avoid small rotary axis motions between successive paths. The optimal ($A^{\text{opt}}_{\text{part}}$,$C^{\text{opt}}_{\text{part}}$) solution for the workpiece is thus defined by (Equation 25).

$$\mathbf{f}^{\text{opt}}_{\text{part}} = \frac{\sum_i \mathbf{f}^{\text{mean}}_{\text{path i}} \Delta s_{\text{path i}}}{\sum_i \Delta s_{\text{path i}}} \quad i \in [\![1; \text{number of paths}]\!] \tag{25}$$

This solution is still close to the optimal solution as long as the surface remains sufficiently stretched despite

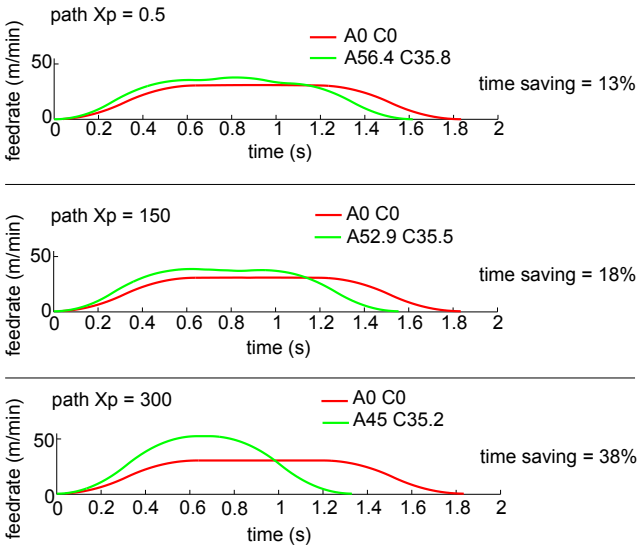

Fig. 20 Measured relative feedrate on three paths for each orientation solution $\mathbf{f}^{\text{mean}}_{\text{path i}}$

the curvature variations. Table 4 compares the total machining time recorded on the Mikron machine for the different orientation optimization strategies.

Table 4 Comparison of total machining time depending on the orientation solution

Strategies	Machining time	Time saving
Basic orientation ($A = 0$,$C = 0$)	36 min 15 s	–
Jerk polytope solution by path $\mathbf{f}^{\text{mean}}_{\text{path i}}$	32 min 30 s	10%
Jerk polytope optimization whole part $\mathbf{f}^{\text{opt}}_{\text{part}}$	30 min 4 s	17%

Machining time is less important for the jerk orientation whereas on each path machining time is smaller. A waste of time is caused by the required time to change the orientation between each path. If the part is bigger, time saving on each path would be more important and so machining time would be reduced. Thus, this method provides greater benefits on long and stretched surfaces.

6 Conclusion

This paper presents a method to optimize the workpiece setup and the tool axis orientation along the path in 3+2-axis machining. The novelty of the paper consists in the approach and method that takes advantage of the use of kinematic manipulability polytope to take into account velocity, acceleration and jerk constraints. The tool axis orientations are computed in order to optimize tangential jerk which is the most limiting parameter to increase the actual feedrate. The two freeform surfaces machined on an industrial milling center illustrate the efficiency of the approach. The recordings of the actual tool feedrate made by the CNC when executing the program show that it is possible to reach the programmed cutting conditions faster. The feedrate is therefore higher along the path, thus reducing the machining time by up to 17% on the large freeform surface. To conclude, kinematic performances of the axes are better used to improve productivity.

However, this gain in feedrate level and machining time must be balanced against the behaviour of the axes and tool. Axis jerk levels as well as a relative tool-part tangential jerk parameter must be set and tuned to contain both the potential vibrations due to axis dynamics or tool vibrations due to cutting loads variations. Adjusting the maximum acceleration and jerk levels remains fundamental to achieving the desired part quality.

In addition, this polytope-based approach provides the user with a graphical interface to optimize processes and understand the optimized results in a much more intuitive way than manipulating complex equations. This would allow an easier integration of kinematic constraints in the choice of machining strategies in CAM software that still do not take these constraints into account so far.

Based on polytopes modelling and the method of resolution demonstrated in 3+2 -axis machining, the long-term objective is to define continuous 5-axis tool paths to take into account kinematic and geometrical constraints of the machine structure. The challenge is then to build a new machining strategy that maximizes kinematics by calculating the tool tip path and tool orientation. It will then be possible to fully exploit the combined effect of the 5 axes of the machine.

A Part orientation solution

The Equation 18 can be detailed as the system of equations:

$$\ddot{q}_x \cos C - \ddot{q}_y \cos A \sin C + \ddot{q}_z \sin A \sin C = \|\ddot{\mathbf{q}}\| f_x \quad (26)$$

$$\ddot{q}_x \sin C + \ddot{q}_y \cos A \cos C - \ddot{q}_z \sin A \cos C = \|\ddot{\mathbf{q}}\| f_y \quad (27)$$

$$\ddot{q}_y \sin A + \ddot{q}_z \cos A = \|\ddot{\mathbf{q}}\| f_z \quad (28)$$

$$\text{with} \quad \ddot{\mathbf{q}} = \begin{bmatrix} \ddot{q}_x \\ \ddot{q}_y \\ \ddot{q}_z \end{bmatrix} \quad \text{and} \quad \mathbf{f}_{\text{path}} = \begin{bmatrix} f_x \\ f_y \\ f_z \end{bmatrix}$$

Equation 28 has the general form:

$$X \sin A^{\text{sol}} + Y \cos A^{\text{sol}} = Z \quad (29)$$

whose solutions are:

$$A^{\text{sol}} = \begin{cases} \text{singular configuration} & \text{if } X = 0 \text{ and } Y = 0 \\ \text{atan2}\left(\pm\sqrt{1-\dfrac{Z^2}{Y^2}}, \dfrac{Z}{Y}\right) & \text{if } X = 0 \text{ and } Y \neq 0 \\ \text{atan2}\left(\dfrac{Z}{X}, \pm\sqrt{1-\dfrac{Z^2}{X^2}}\right) & \text{if } X \neq 0 \text{ and } Y = 0 \\ \text{atan2}(-Y, X)\,[\pi] & \text{if } X \neq 0 \text{ and } Y \neq 0 \text{ and } Z = 0 \\ \text{atan2}\big(\sin A^{\text{sol}}, \cos A^{\text{sol}}\big) & \text{if } X \neq 0 \text{ and } Y \neq 0 \text{ and } Z \neq 0 \text{ and } X^2+Y^2 \geq Z^2 \end{cases} \quad (30)$$

with in the last case:

$$\begin{cases} \cos A^{\text{sol}} = \dfrac{YZ - \varepsilon X\sqrt{X^2+Y^2-Z^2}}{X^2+Y^2} \\ \sin A^{\text{sol}} = \dfrac{XZ + \varepsilon Y\sqrt{X^2+Y^2-Z^2}}{X^2+Y^2} \end{cases} \quad \text{with } \varepsilon = \pm 1 \quad (31)$$

Then Equations 26 and 27 become a system to evaluate C^{sol}:

$$\begin{cases} X_1 \sin C^{\text{sol}} + Y_1 \cos C^{\text{sol}} = Z_1 \\ X_2 \sin C^{\text{sol}} + Y_2 \cos C^{\text{sol}} = Z_2 \end{cases} \quad (32)$$

whose solutions are:

$$C^{\text{sol}} = \begin{cases} \text{atan2}\left(\dfrac{Z_1}{X_1}, \dfrac{Z_2}{Y_2}\right) & \text{if } Y_1 = 0 \text{ and } X_2 = 0 \\ \text{atan2}\big(\sin A^{\text{sol}}, \cos A^{\text{sol}}\big) & \text{if } X_1Y_2 - X_2Y_1 \neq 0 \end{cases} \quad (33)$$

with in the last case:

$$\begin{cases} \cos C^{\text{sol}} = \dfrac{Z_2X_1 - Z_1X_2}{X_1Y_2 - X_2Y_1} \\ \sin C^{\text{sol}} = \dfrac{Z_1Y_2 - Z_2Y_1}{X_1Y_2 - X_2Y_1} \end{cases} \quad (34)$$

B Hyperbolic paraboloid surface

The surface is a Bezier patch of degree (2,2) defined by Equation 35.

$$\mathbf{S}(u,v) = \sum_{i=0}^{2}\sum_{j=0}^{2} B_{i2}(u)\, B_{j2}(v)\, \mathbf{P}_{ij} \quad (u,v) \in [0,1]^2 \quad (35)$$

with $B_{im}(u)$ the Bernstein function

$$B_{im}(u) = \frac{m!}{i!\,(m-i)!}\, u^i\, (1-u)^{m-i} \quad (36)$$

and $\mathbf{P}_{ij}$ the control points:

$$\mathbf{P}_{00} = \begin{bmatrix} -50 \\ -50 \\ 0 \end{bmatrix} \quad \mathbf{P}_{01} = \begin{bmatrix} -50 \\ 0 \\ -10 \end{bmatrix} \quad \mathbf{P}_{02} = \begin{bmatrix} -50 \\ 50 \\ 0 \end{bmatrix}$$

$$\mathbf{P}_{10} = \begin{bmatrix} 0 \\ -50 \\ 10 \end{bmatrix} \quad \mathbf{P}_{11} = \begin{bmatrix} 0 \\ 0 \\ 0 \end{bmatrix} \quad \mathbf{P}_{12} = \begin{bmatrix} 0 \\ 50 \\ 10 \end{bmatrix}$$

$$\mathbf{P}_{20} = \begin{bmatrix} 50 \\ -50 \\ 0 \end{bmatrix} \quad \mathbf{P}_{21} = \begin{bmatrix} 50 \\ 0 \\ -10 \end{bmatrix} \quad \mathbf{P}_{22} = \begin{bmatrix} 50 \\ 50 \\ 0 \end{bmatrix}$$

C Definition of the Manta surface

Manta surface is a Bezier patch of degree (3,3) defined by Equation 37.

$$\mathbf{S}(u,v) = \sum_{i=0}^{3}\sum_{j=0}^{3} B_{i3}(u)\, B_{j3}(v)\, \mathbf{P}_{ij} \quad (u,v) \in [0,1]^2 \quad (37)$$

with following $\mathbf{P}_{ij}$ control points:

$$\mathbf{P}_{00} = \begin{bmatrix} 0 \\ 0 \\ 0 \end{bmatrix} \quad \mathbf{P}_{01} = \begin{bmatrix} 0 \\ 200 \\ 0 \end{bmatrix} \quad \mathbf{P}_{02} = \begin{bmatrix} 0 \\ 400 \\ 100 \end{bmatrix} \quad \mathbf{P}_{03} = \begin{bmatrix} 0 \\ 600 \\ 100 \end{bmatrix}$$

$$\mathbf{P}_{10} = \begin{bmatrix} 200 \\ 0 \\ 0 \end{bmatrix} \quad \mathbf{P}_{11} = \begin{bmatrix} 200 \\ 200 \\ 0 \end{bmatrix} \quad \mathbf{P}_{12} = \begin{bmatrix} 200 \\ 400 \\ 100 \end{bmatrix} \quad \mathbf{P}_{13} = \begin{bmatrix} 200 \\ 600 \\ 100 \end{bmatrix}$$

$$\mathbf{P}_{20} = \begin{bmatrix} 400 \\ 0 \\ 100 \end{bmatrix} \quad \mathbf{P}_{21} = \begin{bmatrix} 400 \\ 200 \\ 100 \end{bmatrix} \quad \mathbf{P}_{22} = \begin{bmatrix} 400 \\ 400 \\ 0 \end{bmatrix} \quad \mathbf{P}_{23} = \begin{bmatrix} 400 \\ 600 \\ 0 \end{bmatrix}$$

$$\mathbf{P}_{30} = \begin{bmatrix} 600 \\ 0 \\ 100 \end{bmatrix} \quad \mathbf{P}_{31} = \begin{bmatrix} 600 \\ 200 \\ 100 \end{bmatrix} \quad \mathbf{P}_{32} = \begin{bmatrix} 600 \\ 400 \\ 0 \end{bmatrix} \quad \mathbf{P}_{33} = \begin{bmatrix} 600 \\ 600 \\ 0 \end{bmatrix}$$

Declarations

Ethical Approval

Not applicable. This study does not involve human participants nor animals.

Consent to Participate

Not applicable. This study does not involve human subjects.

Consent to Publish

Not applicable. This study does not involve human subjects.

Authors Contributions

The submitted work is original and has not been published elsewhere in any form or language.

Funding

No funds, grants, or other support was received for conducting this study and for the submitted work.

Competing Interests

All authors certify that they have no affiliations with or involvement in any organization or entity with any financial interest or non-financial interest in the subject matter or materials discussed in this manuscript.

Availability of data and materials

No other supplementary files to be published online.

References

1. Gupta P, Janardan R, Majhi J, Woo T (1996) Efficient geometric algorithms for workpiece orientation in 4- and 5-axis NC machining. Comput -Aided Des 28(8):577 – 587, DOI 10.1016/0010-4485(95)00071-2
2. Kang JK, Suh SH (1997) Machinability and set-up orientation for five-axis numerically controlled machining of free surfaces. The Int J of Adv Manuf Technol 13(5):311–325, DOI 10.1007/BF01178251
3. Tang K, Chen LL, Chou SY (1998) Optimal workpiece setups for 4-axis numerical control machining based on machinability. Comput in Ind 37(1):27 – 41, DOI 10.1016/S0166-3615(98)00067-0
4. Hu P, Tang K, Lee CH (2013) Global obstacle avoidance and minimum workpiece setups in five-axis machining. Comput -Aided Des 45(10):1222 – 1237, DOI 10.1016/j.cad.2013.05.007
5. Chiou CJ, Lee YS (2002) A machining potential field approach to tool path generation for multi-axis sculptured surface machining. Comput -Aided Des 34(5):357 – 371, DOI 10.1016/S0010-4485(01)00102-6
6. Barakchi Fard MJ, Feng HY (2010) Effective Determination of Feed Direction and Tool Orientation in Five-Axis Flat-End Milling. J of Manuf Sci and Eng 132(6), DOI 10.1115/1.4002766
7. Zębala W, Plaza M (2014) Comparative study of 3- and 5-axis CNC centers for free-form machining of difficult-to-cut material. Int J of Prod Econ 158:345–358, DOI 10.1016/j.ijpe.2014.08.006
8. Kim T, Sarma SE (2002) Toolpath generation along directions of maximum kinematic performance; a first cut at machine-optimal paths. Comput -Aided Des 34(6):453 – 468, DOI 10.1016/S0010-4485(01)00116-6
9. Farouki RT, Han CY, Li S (2014) Inverse kinematics for optimal tool orientation control in 5-axis CNC machining. Comput Aided Geom Des 31(1):13 – 26, DOI doi.org/10.1016/j.cagd.2013.11.002
10. Hu P, Chen L, Tang K (2017) Efficiency-optimal isoplanar tool path generation for five-axis finishing machining of freeform surfaces. Comput -Aided Des 83:33 – 50, DOI doi.org/10.1016/j.cad.2016.10.001
11. Bohez ELJ (2002) Five-axis milling machine tool kinematic chain design and analysis. Int J of Mach Tools and Manuf 42(4):505 – 520, DOI 10.1016/S0890-6955(01)00134-1
12. Tutunea-Fatan OR, Feng HY (2004) Configuration analysis of five-axis machine tools using a generic kinematic model. Int J of Mach Tools and Manuf 44(11):1235 – 1243, DOI 10.1016/j.ijmachtools.2004.03.009
13. Anotaipaiboon W, Makhanov S, Bohez E (2006) Optimal setup for five-axis machining. Int J of Mach Tools and Manuf 46(9):964 – 977, DOI 10.1016/j.ijmachtools.2005.07.046
14. Lin Z, Fu J, Shen H, Gan W (2014) On the workpiece setup optimization for five-axis machining with RTCP function. The Int J of Adv Manuf Technol 74(1):187–197, DOI 10.1007/s00170-014-5981-6
15. Yang J, Aslan D, Altintas Y (2018) Identification of workpiece location on rotary tables to minimize tracking errors in five-axis machining. Int J of Mach Tools and Manuf 125:89 – 98, DOI 10.1016/j.ijmachtools.2017.11.009
16. Pessoles X, Landon Y, Segonds S, Rubio W (2013) Optimisation of workpiece setup for continuous five-axis milling: application to a five-axis BC type machining centre. The Int J of Adv Manuf Technol 65(1):67–79, DOI 10.1007/s00170-012-4151-y
17. Shaw D, Ou GY (2008) Reducing X,Y and Z axes movement of a 5-axis AC type milling machine by changing the location of the work-piece. Comput -Aided Des 40(10):1033 – 1039, DOI 10.1016/j.cad.2008.09.001
18. Dong J, Ferreira PM, Stori JA (2007) Feed-rate optimization with jerk constraints for generating minimum-time trajectories. Int J of Mach Tools and Manuf 47(12):1941 – 1955, DOI 10.1016/j.ijmachtools.2007.03.006
19. Sencer B, Altintas Y, Croft E (2008) Feed optimization for five-axis CNC machine tools with drive constraints. Int J of Mach Tools and Manuf 48(7):733 – 745, DOI 10.1016/j.ijmachtools.2008.01.002
20. Bosetti P, Bertolazzi E (2014) Feed-rate and trajectory optimization for CNC machine tools. Robot and Comput -Integr Manuf 30(6):667 – 677, DOI 10.1016/j.rcim.2014.03.009
21. Hu P, Tang K (2011) Improving the dynamics of five-axis machining through optimization of workpiece setup and tool orientations. Comput -Aided Des 43(12):1693–1706, DOI 10.1016/j.cad.2011.09.005
22. Xu K, Tang K (2016) Optimal workpiece setup for time-efficient and energy-saving five-axis machining of freeform surfaces. J of Manuf Sci and Eng 139(5), DOI 10.1115/1.4034846
23. Campatelli G, Scippa A, Lorenzini L, Sato R (2015) Optimal workpiece orientation to reduce the energy consumption of a milling process. Int J of Precis Eng and Manuf -Green Technol 2(1):5–13, DOI 10.1007/s40684-015-0001-3
24. Zhu Y, Chen ZT, Ning T, Xu RF (2016) Tool orientation optimization for 3+2-axis CNC machining of sculptured surface. Comput -Aided Des 77:60–72, DOI 10.1016/j.cad.2016.02.007
25. Vulliez M, Lavernhe S, Bruneau O (2017) Dynamic approach of the feedrate interpolation for trajectory planning process in multi-axis machining. The Int J of Adv Manuf Technol 88(5):2085–2096, DOI 10.1007/s00170-016-8903-y
26. Erkorkmaz K, Altintas Y (2001) High speed CNC system design. part I: jerk limited trajectory generation and quintic spline interpolation. Int J of Mach Tools and Manuf 41(9):1323–1345, DOI 10.1016/S0890-6955(01)00002-5
27. Yoshikawa T (1985) Manip of robot mech. The International Journal of Robotics Research 4(2):3–9, DOI 10.1177/027836498500400201
28. Merlet JP (2005) Jacobian, Manipulability, Condition Number, and Accuracy of Parallel Robots. J of Mech Des 128(1):199–206, DOI 10.1115/1.2121740
29. Briot S, Pashkevich A, Chablat D (2010) Optimal technology-oriented design of parallel robots for high-speed machining applications. In: 2010 IEEE Int Conf on Robot and Autom, pp 1155–1161, DOI 10.1109/ROBOT.2010.5509543
30. Fukuda K (2004) From the zonotope construction to the minkowski addition of convex polytopes. J of Symb Comput 38(4):1261 – 1272, DOI 10.1016/j.jsc.2003.08.007, symbolic Computation in Algebra and Geometry

31. Ziegler GM (1995) Lectures on Polytopes, Graduate Texts in Mathematics, vol 152. Springer-Verlag New York, DOI 10.1007/978-1-4613-8431-1